Princeton Plasma Physics Laboratory

PPPL- 4315

PPPL- 4315

Error Field Correction in ITER

Jong-kyu Park, Allen H. Boozer,
Jonathan E. Menard, and Michael J. Schaffer

May 2008

Prepared for the U.S. Department of Energy under Contract DE-AC02-76CH03073.

Princeton Plasma Physics Laboratory
Report Disclaimers

Full Legal Disclaimer

Trademark Disclaimer

PPPL Report Availability

Princeton Plasma Physics Laboratory:

http://www.pppl.gov/techreports.cfm

Office of Scientific and Technical Information (OSTI):

http://www.osti.gov/bridge

Related Links:

U.S. Department of Energy

Office of Scientific and Technical Information

Fusion Links

Error Field Correction in ITER

Jong-kyu Park,[1] Allen H. Boozer,[2] Jonathan E. Menard,[1] and Michael J. Schaffer[3]

[1]*Princeton Plasma Physics Laboratory, Princeton, New Jersey, NJ 08543*
[2]*Department of Applied Physics and Applied Mathematics, Columbia University, New York, NY 10027*
[3]*General Atomics, San Diego, CA 92186*

(Dated: February 24, 2008)

A new method for correcting magnetic field errors in the ITER tokamak is developed using the Ideal Perturbed Equilibrium Code (IPEC). The dominant external magnetic field for driving islands is shown to be localized to the outboard midplane for three ITER equilibria that represent the projected range of operational scenarios. The coupling matrices between the poloidal harmonics of the external magnetic perturbations and the resonant fields on the rational surfaces that drive islands are combined for different equilibria and used to determine an ordered list of the dominant errors in the external magnetic field. It is found that efficient and robust error field correction is possible with a fixed setting of the correction currents relative to the currents in the main coils across the range of ITER operating scenarios that was considered.

I. INTRODUCTION

Tokamaks are highly sensitive to magnetic perturbations that break toroidal symmetry [1–4]. Such perturbations always exist due to imperfections in magnetic field coils or the presence of magnetic materials. Locked modes arise in tokamaks when the external perturbing field has a sufficient amplitude to overcome plasma shielding effects. Magnetic islands can then abruptly open on the rational magnetic surfaces $\psi = \psi_{mn}$, where the safety factor $q(\psi_{mn}) = m/n$ with m a poloidal and n a toroidal mode number of a Fourier component of the magnetic perturbation. Locking can occur with perturbations as small as $|\delta\vec{B}|/|\vec{B}| \approx 10^{-4}$ and can lead to the destruction of the plasma equilibrium, called a disruption. Since locked modes are a direct consequence of asymmetric magnetic fields, success in error field correction is often measured by the mitigation of locked modes.

In principle it would be better to eliminate any magnetic field error that breaks the toroidal symmetry, but in practice only parts of the intrinsic error field can be eliminated directly. Currents in a limited set of error field correction coils can be used to remove the dominant spatial distributions of the error field on the plasma boundary. In other words, not all magnetic field distributions that break the toroidal symmetry are equally important in producing locked modes, and the dominant one can be removed by currents in an appropriate set of error field correction coils.

The sensitivity of plasmas to symmetry breaking magnetic fields has been studied in the limit of a cylindrical plasma [5, 6], and this theory has been the basis of a number of experiments [4, 7–12]. A cylindrical, unlike a toroidal, plasma has no coupling between the poloidal harmonics m. To address the mode coupling that arises in a torus, the three mode coupling method has been developed [8, 13], but even the coupling of three modes $(m, m\pm1)$ does not explain the behavior of a locked mode at the rational surface $q = m/n$ in a tokamak [14].

A salient feature of mode locking in tokamaks is that the external field that drives islands is highly localized near the outboard midplane [14]. This localization gives a strong coupling of the various poloidal Fourier modes of the perturbation but actually simplifies the design of appropriate error field correction coils. The localization is sufficiently robust that a set of error field correction coils with settings fixed to the currents in the primary coils can correct the dominant field errors over a large range of plasma equilibria.

The resonant magnetic field that drives an island on a rational surface $q = m/n$ comes not only from external currents that break the toroidal symmetry but also from the perturbed plasma current that arises from the distortion in the path of the currents associated with the plasma equilibrium. In other words, the determination of the resonant field that arises in response to a given external magnetic field error requires the calculation of the perturbed plasma equilibrium, $\vec{\nabla}\delta p = \vec{j} \times \delta\vec{B} + \delta\vec{j} \times \vec{B}$. An equilibrium with the magnetic surfaces perturbed by a distance $\vec{\xi}$, while preserving the safety factor $q(\psi)$ and pressure $p(\psi)$ profiles, is found by letting $\delta\vec{j} = (\vec{\nabla} \times \delta\vec{B})/\mu_0$, $\delta\vec{B} = \vec{\nabla} \times (\vec{\xi} \times \vec{B})$ and $\delta p = -\vec{\xi} \cdot \vec{\nabla} P - \gamma P(\vec{\nabla} \cdot \vec{\xi})$.

This description of perturbations is used in ideal magnetohydrodynamics (MHD) stability codes such as DCON [15]. The Ideal Perturbed Equilibrium Code (IPEC) [16] augments the DCON and VACUUM [17] code by finding the externally produced field normal to plasma boundary, $\delta\vec{B}^x_j \cdot \hat{n}_b$ that is associated with the j^{th} field perturbation $\delta\vec{B}_j(\vec{x})$ and the displacement $\vec{\xi}_j(\vec{x})$, which satisfy the perturbed equilibrium equations. DCON finds a set of $\delta\vec{B}_j(\vec{x})$, $1 \le j \le M$, that can describe all the perturbations for each toroidal mode n within the range of retained poloidal mode number M. This set is essentially the set of eigenmodes minimizing plasma potential energy $\delta W_p(\vec{\xi})$. Here one must distinguish between the external field, $\delta\vec{B}^x$, produced by external coils and the total field, $\delta\vec{B}$, produced by currents both in the plasma and external coils. If the actual exter-

nal field $\delta\vec{B}^x\cdot\hat{n}_b$ is expanded as $\delta\vec{B}^x\cdot\hat{n}_b=\sum_j c_j\delta\vec{B}^x_j\cdot\hat{n}_b$ then the actual field and displacement are $\delta\vec{B}(\vec{x})=\sum_j c_j\delta\vec{B}_j(\vec{x})$ and $\vec{\xi}(\vec{x})=\sum_j c_j\vec{\xi}_j(\vec{x})$. In other words, given the normal magnetic field on the plasma boundary due to currents external to the plasma, $\delta\vec{B}^x\cdot\hat{n}_b$, IPEC finds the perturbed magnetic field due to both plasma and external currents $\delta\vec{B}(\vec{x})$ throughout the plasma volume.

When a plasma is perturbed in a way that preserves the $q(\psi)$ profile, as in ideal MHD, surface currents must arise on the rational surfaces $q=m/n$ to prevent islands from opening, for islands would change the q profile. The constraint of no islands implies that the Fourier component $(\delta\vec{B}\cdot\vec{\nabla}\psi/\vec{B}\cdot\vec{\nabla}\varphi)_{mn}$ in magnetic angles must vanish, where φ is the toroidal angle. The surface current that arises on the rational surface $q=m/n$ to ensure that this Fourier component vanishes produces a discontinuity in the perturbed tangential field across the rational surface. Since $\vec{\nabla}\cdot\delta\vec{B}=0$, this discontinuity can be measured by the dimensionless quantity [18]

$$\Delta_{mn}\equiv\left[\frac{\partial}{\partial\psi}\frac{\delta\vec{B}\cdot\vec{\nabla}\psi}{\vec{B}\cdot\vec{\nabla}\varphi}\right]_{mn}, \tag{1}$$

where ψ is the poloidal flux and (θ,φ) are magnetic angles. The $[\cdots]_{mn}$ denotes the jump in the resonant component. The surface current associated with the discontinuity in the tangential field is

$$\vec{j}_{smn}=i\frac{\Delta_{mn}me^{i(m\theta-n\varphi)}}{\mu_0 n^2(\oint dSB^2/|\vec{\nabla}\psi|^3)}\delta(\psi-\psi_{mn})\vec{B}. \tag{2}$$

The surface current $\vec{j}_{smn}$ of ideal MHD produces a resonant normal field, denoted by $-(\delta\vec{B}\cdot\hat{n})_{mn}$. This field would form a magnetic island if the singular current were dissipated and is a critical measure of the drive for mode locking and of the magnitude of the toroidal torque that the perturbation can produce [19]. The total resonant field $(\delta\vec{B}\cdot\hat{n})_{mn}$ is generally very different from that produced by the currents external to the plasma alone, or the external (vacuum) resonant field, $(\delta\vec{B}^x\cdot\hat{n})_{mn}$. For the dominant error fields, the distorted path of the plasma equilibrium currents is a larger contributor to $(\delta\vec{B}\cdot\hat{n})_{mn}$ than the direct effect of the currents external to the plasma.

The present design of ITER has a set of slow coils for error field correction. Such coils are most effective if a fixed setting of the currents in the correction coils relative to the currents in the main coils suffices over the expected range [20] of ITER pressure and current profiles, Fig. 1. This paper explains how correction coils can be chosen to have this property.

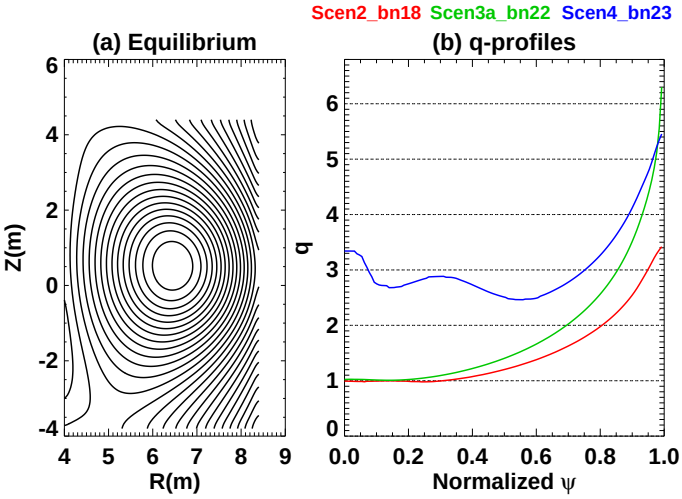

FIG. 1: (a) Flux surfaces of the equilibrium in the ITER hybrid scenario (Scen3a-bn22) and (b) q profiles of the equilibria of the inductive (Scen2-bn18, red), hybrid (Scen3a-bn22, green) and advanced (Scen4-bn23, blue) scenarios. The 'bn' denotes a β_n value.

II. RELATIVE IMPORTANCE OF ERROR FIELDS

Magnetic fields produced by currents external to the plasma boundary can be characterized by the spatial distribution of normal magnetic field they produce on the plasma boundary. For a given plasma equilibrium, IPEC together with Singular Value Decomposition (SVD) can be used to find the unique normalized spatial distribution of external normal field that dominantly drives the total resonant field $(\delta\vec{B}\cdot\hat{n})_{mn}$, in other words, maximizes the $(\delta\vec{B}\cdot\hat{n})_{mn}$ at a particular rational surface for a given $\oint(\delta\vec{B}^x\cdot\hat{n})^2da$ on the plasma boundary. The procedure for doing this is explained in this section. When this is done, one finds this unique distribution of external normal field is almost the same (1) for all the rational surfaces with a given toroidal mode number n and (2) for essentially all plasma equilibria.

The implication of the dominant distribution of external normal field of given n being almost independent of the rational surface and the equilibrium being considered is that a global error field correction is possible. Given a collection of equilibria and a set of rational surfaces, SVD methods can determine a set of normal magnetic field distributions on a control surface that are ordered by the efficiency with which they drive $(\delta\vec{B}\cdot\hat{n})_{mn}$'s at the rational surfaces. By designing error field control coils to null the dominant external magnetic perturbations, one can greatly reduce the sensitivity of a tokamak to field errors with a simple coil set that has fixed currents relative to the currents in the primary field coils. This procedure for designing such coils and quantifying their benefits will be given in the next section.

An externally produced error field can be decomposed

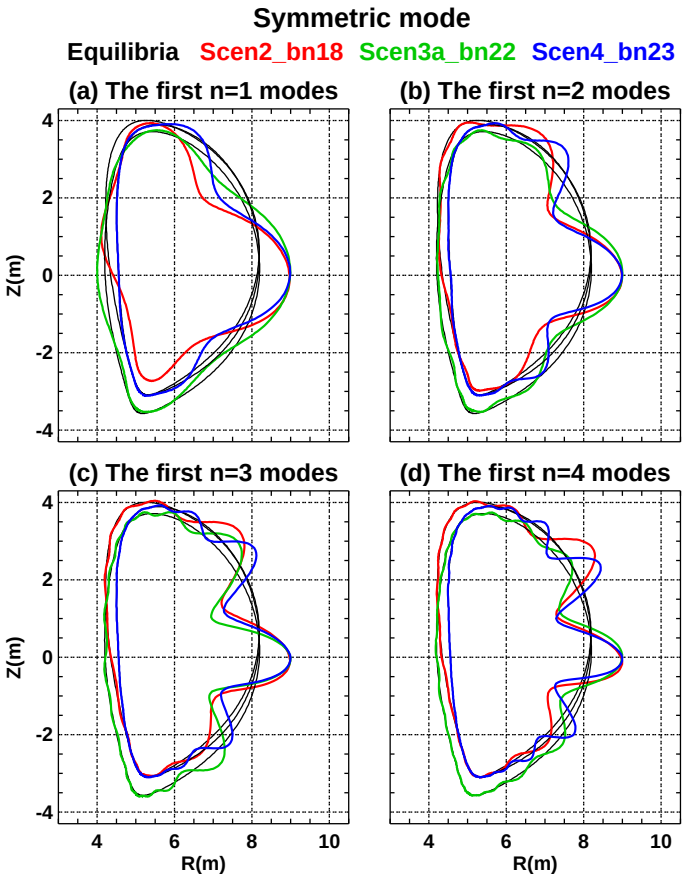

FIG. 2: The up-down symmetric part of the dominant external field relative to the plasma boundary of the three equilibria for (a) $n = 1$ (b) $n = 2$ (c) $n = 3$ (d) $n = 4$ toroidal harmonics. Note the localization of the first mode driving the total resonant field.

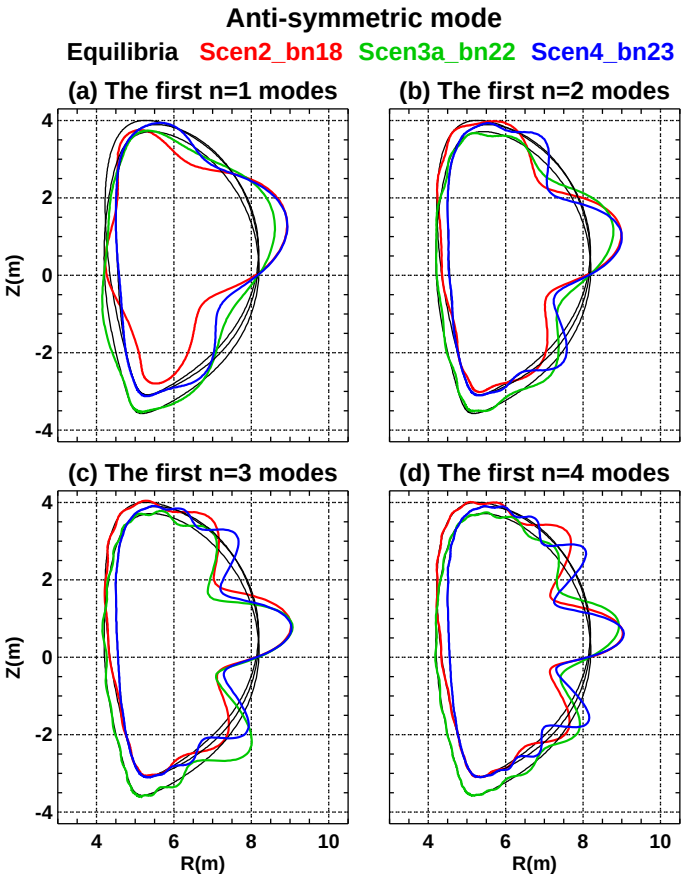

FIG. 3: The up-down anti-symmetric part of the dominant external field relative to the plasma boundary of the three equilibria for (a) $n = 1$ (b) $n = 2$ (c) $n = 3$ (d) $n = 4$ toroidal harmonics. Also note the localization of the first mode driving the total resonant field.

on the plasma boundary as

$$(\delta\vec{B}^x \cdot \hat{n}_b)(\theta,\varphi) = Re\left(\sum_m \Phi^x_{mn} w(\theta) e^{i(m\theta - n\varphi)}\right), \quad (3)$$

for each toroidal harmonic n. Here $\hat{n}_b$ is the unit vector normal to the plasma boundary and the weight function $w(\theta) = 1/|\mathcal{J}\vec{\nabla}\psi|$ with $\mathcal{J}(\theta)$ the Jacobian of (ψ,θ,φ) coordinates. The Fourier expansion coefficients Φ^x_m, which have units of magnetic flux, constitute a matrix vector $\vec{\Phi}^x$ for each toroidal mode number n. By finding the perturbed equilibrium given by each Fourier component Φ^x_m, one can obtain the total resonant field at each rational surface $(\delta\vec{B}\cdot\hat{n})_{mn}$. This set of Fourier coefficients can also be represented as a matrix vector $\vec{\mathcal{B}}$, which is related to the flux matrix vector by

$$\vec{\mathcal{B}} = \overleftrightarrow{\mathcal{C}} \cdot \vec{\Phi}^x. \quad (4)$$

The coupling matrix $\overleftrightarrow{\mathcal{C}}$ has dimensions $R \times M$,where R is the number of rational surfaces included and M is the number of retained poloidal harmonics of the external error field on the boundary. If only one rational surface is retained $R = 1$, then an SVD analysis of Eq. (4) gives the unique distribution of external normal field on the plasma boundary that drives an island on the rational surface. Other normal field distributions on the plasma boundary have no effect on islands at that rational surface in a linear perturbation analysis.

When Eq. (4) is used to find the distribution of normal magnetic field that drives the island at a particular rational surface, one obtains a very similar answer regardless of which rational surface is considered–at least for rational surfaces ψ_{mn} that are further from the edge than $\psi_{mn}/\psi_{total} < 0.9$. The total resonant fields $(\delta\vec{B}\cdot\hat{n})_{mn}$ near the edge have small influence on the bulk of the plasma, so are neglected here. If $\vec{\mathcal{B}}$ includes all R rational surfaces that lie in the region $\psi_{mn}/\psi_{total} < 0.9$, then an SVD analysis gives R distributions of external normal magnetic field on the plasma surface ranked by their effectiveness in coupling through the plasma to drive magnetic islands at all the rational surfaces in the region, $\psi_{mn}/\psi_{total} < 0.9$. In the conventional treatment for locking, a particular rational surface such as $q = 2$ is typically

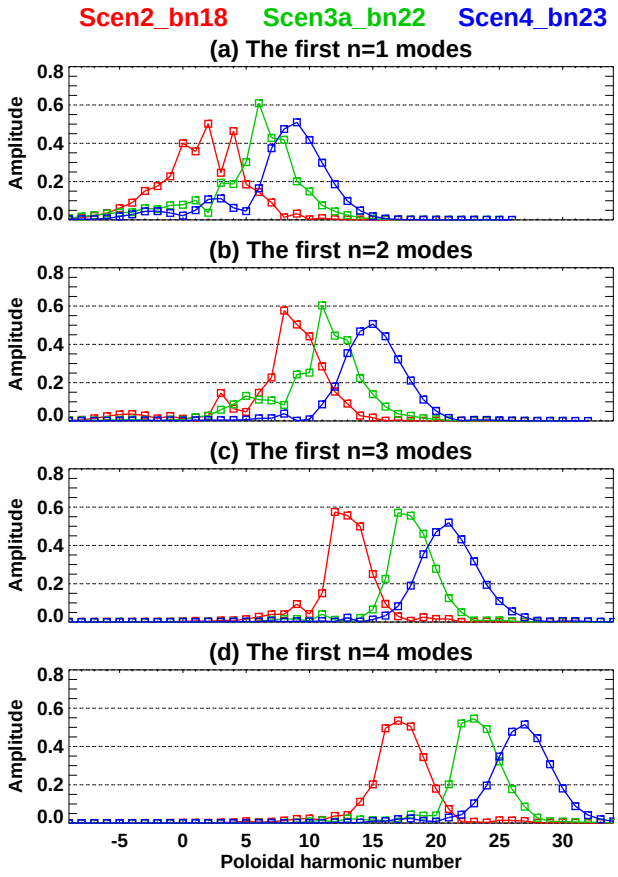

FIG. 4: Coupling spectrum between the resonant field on rational surfaces and poloidal harmonics m of the dominant external field on the plasma boundary for three equilibria and for (a) $n = 1$ (b) $n = 2$ (c) $n = 3$ (d) $n = 4$ toroidal harmonics. The poloidal harmonics are decomposed in Hamada coordinates [21].

considered based on experimental observations. This is true if plasma has monotonically increasing q-profile with $q > 1$, then lowest shear in $q = 2$ makes the surface more vulnerable even with the same amount of $(\delta\vec{B} \cdot \hat{n})_{mn}$. However, including many rational surfaces enables one to estimate error field effects in a more conservative way. Plasmas that represent the three operating scenarios of ITER are somewhat different from conventional plasmas since they are heavily optimized for better confinement. Moreover, the dominant mode for all rational surfaces is almost the same as the dominant mode for one particular rational surface in $\psi_{mn}/\psi_{total} < 0.9$.

Each of the R external field distributions that are analyzed with the R rational surface can be defined as a i^{th} mode of external normal magnetic field. Each is a mixture of poloidal harmonics and is very different from what is expected in cylinder because of the strong poloidal coupling [14]. Each of these distributions of the externally produced magnetic field can be described as $\delta\vec{B}^x \cdot \hat{n}_b = C(\theta)\cos(n\phi) \pm S(\theta)\sin(n\phi)$, where ϕ is the cylindrical toroidal angle, not the magnetic angle φ. The spatial structure of external error field corresponding to each mode can be described by plotting a curve that deviates from the plasma boundary by an amount proportional to the up-down symmetric part $C(\theta)$ and the anti-symmetric part $S(\theta)$.

The $C(\theta)$ of the dominant external field error is plotted in Fig. 2 and the $S(\theta)$ in Fig 3, for three representative ITER equilibria with the toroidal mode numbers n between 1 and 4. The localization of the dominant external field error near the outboard midplane is similar for the three equilibria though some distinctions can be seen in the Fourier decompositions, Fig. 4. The broad coupling spectra over high poloidal harmonics in Fourier space correspond to the highly localized feature in real space as explained in Appendix. The highly localized feature implies that a set of control coils located near the outboard section can control the dominant mode effectively and independently of the equilibria provided the plasma boundary is not markedly changed. In fact, this robustness of the dominant mode has been found in other tokamaks such as NSTX and DIII-D, and verified in plasma locking experiments [14]. In practice, locking can be easily mitigated with the coils located at the outboard midplane and slightly off-midplane, which can compensate most efficiently any part of intrinsic error field overlapped with the $C(\theta)$ and $S(\theta)$ of the dominant mode.

The three equilibria used to construct Figures 2 and 3 are defined by the three operating scenarios being considered for ITER: the inductive, the hybrid and the advanced scenario, which are designated as scenario 2, 3a and 4, respectively in Reference [20]. Fig. 1 shows (a) the flux surfaces of an equilibrium in the hybrid scenario and (b) the three different q profiles of these scenarios. The equilibrium in the inductive scenario has three $q = 1$ surfaces, and the equilibrium in the advanced scenario has two $q = 3$ surfaces but no $q = 2$ surface. Each of these equilibria can be modified by adding a scale factor to the plasma pressure or current profile. IPEC found that the dominant external field error has a spatial distribution that is weakly dependent on such scaling factors. However, the relative scaling between the external field and the resonant field on each rational surface is dependent on the closeness of the equilibrium to the no-wall stability limit. This sensitivity of the relative scaling to the plasma pressure can be parameterized by the normalized beta, $\beta_n \equiv \langle\beta_t\rangle_p / aB_{t0}$, where β_t is the toroidal β, I_p is the plasma current, a is the minor radius, and B_{t0} is the toroidal field at the magnetic axis. In Fig. 2, the normalized beta was chosen so $\beta_n = 1.8, 2.2$, and 2.3 for the inductive, the hybrid, and the advanced scenario respectively. With this choice each equilibrium is stable without a conducting wall, and a comparable energy is required to drive the least stable perturbation.

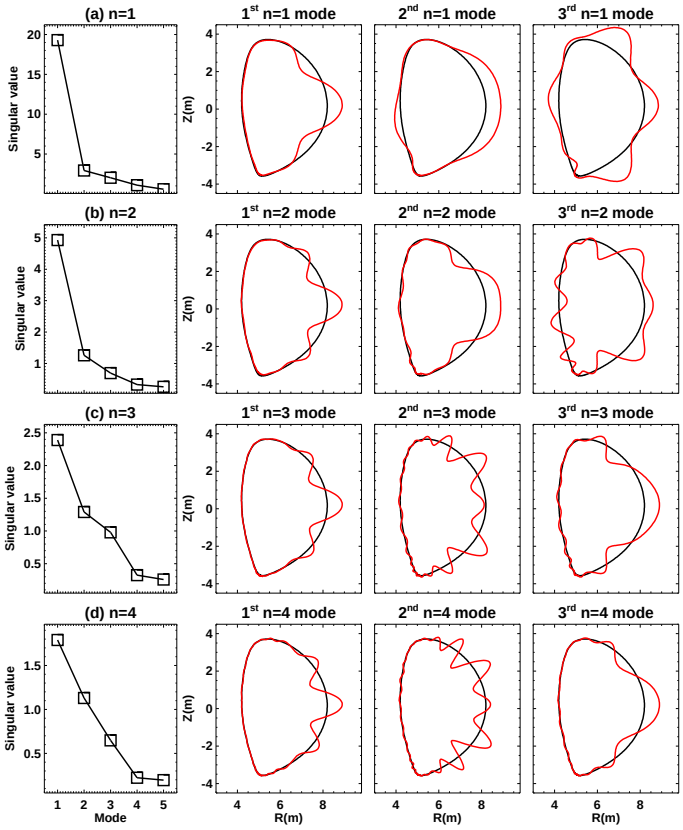

FIG. 5: Singular values of the first five modes (the first column) and the external field of the first three modes (red) of the combined coupling matrix between the resonant field and the external field on a control surface, for (a) $n = 1$ (b) $n = 2$ (c) $n = 3$ (d) $n = 4$ toroidal harmonics. Only the $C(\theta)$ part is shown. The importance of the first mode can be seen from the singular values, which give the average number of Gauss of resonant field on the resonant rational surfaces when the the external flux of the perturbation $|(\delta\vec{B}^x \cdot \hat{n}_b)_{mn}| = 1\,Gauss$. Note that the lower toroidal modes have the larger singular values.

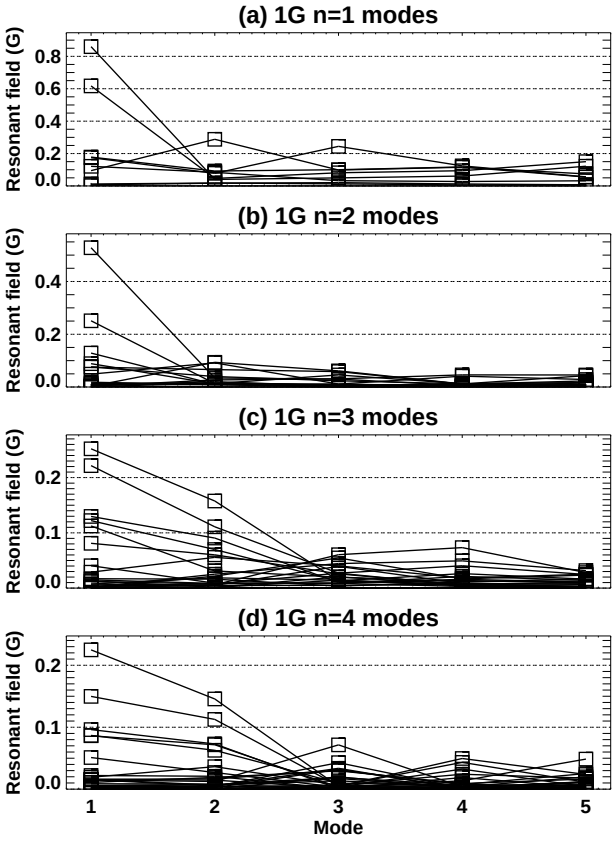

FIG. 6: The total resonant field $(\delta\vec{B} \cdot \hat{n})_{mn}$ on all the rational surfaces in the three ITER equilibria, by each mode having $1\,Gauss$ amplitude in maximum for (a) $n = 1$ (b) $n = 2$ (c) $n = 3$ (d) $n = 4$ toroidal harmonics.

III. GLOBAL CONTROL OF ITER ERROR FIELDS

As discussed in Sec. II, the dominant distribution, or the first mode for the external magnetic field error, can be used to mitigate field errors for each scenario. However, the present design for ITER would require a fixed setting of the current in the correction coils, which has to be effective to minimize the first mode in all probable equilibria in ITER. This global control concept can be designed by combining each coupling matrix $\overleftrightarrow{C}$, and the fact that the first mode is almost independent of the operating scenario makes the global control more effective.

The dominant external field errors in ITER are defined by finding the combined coupling matrix $\overleftrightarrow{C}$ that relates the Fourier coefficients of the external normal field on a control surface and the resonant field on the rational surfaces of the three equilibria that represent the three ITER scenarios. Figure 3 gives the results of the SVD analysis of this combined coupling matrix for $n = 1$ to 4. Here only the symmetric part $C(\theta)$ is shown since $S(\theta)$ is approximated by the derivative of $C(\theta)$. The singular values, which are in the left column of Fig. 4, gives the average number of Gauss of resonant field on the rational surfaces when the the external field of the perturbation $|(\delta\vec{B}^x \cdot \hat{n}_b)_{mn}| = 1\,Gauss$. For the $n = 1$ and the $n = 2$ cases, the largest singular value is 5 to 10 times larger than the next to the largest. A set of coils that can null just the error field to which the plasmas are most sensitive, the dominant $n = 1$ mode already has a large effect. Higher order modes are more difficult to control– both due to their more rapid spatial variation and due to their greater sensitivity to the details of the plasma equilibrium, but their small singular values indicate the insignificance of the higher modes.

To illustrate the benefits of a global error field correction, the total resonant field $(\delta\vec{B} \cdot \hat{n})_{mn}$ at all rational surfaces of three equilibria are investigated when each i^{th} external field is separately applied, for each toroidal mode number n. Each mode is assumed to have the amplitude of $1\,Gauss$ at its maximum. Figure 6 shows all the total resonant field $(\delta\vec{B} \cdot \hat{n})_{mn}$ included in three equi-

libria when applying each of the first five i^{th} modes with $1\,Gauss$ amplitude at its maximum on the boundary. In total, 14, 26, 39 and 52 rational surfaces and $(\delta\vec{B}\cdot\hat{n})_{mn}$ are estimated for each mode, for $n=1$, 2, 3 and 4, respectively. This figure shows that $(\delta\vec{B}\cdot\hat{n})_{mn}$'s become negligible quickly when the rank of the mode increases, even from the second mode for $n=1$ and 2. For higher n, the second mode remains comparable to the first mode, but overall $(\delta\vec{B}\cdot\hat{n})_{mn}$'s become smaller. So one can determine what is the largest $(\delta\vec{B}\cdot\hat{n})_{mn}$ that should be minimized at first, from Fig. 6. In this example, one can find the maximal $(\delta\vec{B}\cdot\hat{n})_{mn}\sim 0.85\,Gauss$ by the first $n=1$ mode in (a). The large $(\delta\vec{B}\cdot\hat{n})_{mn}$ in this calculation is typically at a rational surface having positive q shear in the core region, that is, $q=3$ in the advanced scenario and $q=2$ in the inductive and hybrid scenario.

The results can be placed in perspective by considering that a locked mode might occur when $(\delta\vec{B}\cdot\hat{n})_{mn}\sim 10\,Gauss\ n_e(10^{19}m^{-3})$ with the electron density n_e. The linear scaling with density has been found in many tokamaks [9–11], and the $10\,Gauss$ factor is based on a recent study relating the total resonant field and mode locking in DIII-D [14]. Other parameters for scaling are neglected here since they are not yet systematically studied in terms of the total resonant field $(\delta\vec{B}\cdot\hat{n})_{mn}$. When $n_e=10^{19}m^{-3}$, the external field at the outboard midplane should be reduced below $10/0.85\sim 12\,Gauss$ for $n=1$, $10/0.55\sim 18\,Gauss$ for $n=2$, where 0.85 and 0.55 is the highest $(\delta\vec{B}\cdot\hat{n})_{mn}$ driven by the $1\,Gauss$ $n=1$ and $n=2$ mode at its maximum, respectively. The maximum occurs at the outboard midplane for the $C(\theta)$ of the first mode. This is somewhat conservative since locking density has been expected to have roughly a linear R, major radius, scaling. The detailed locking scaling using $(\delta\vec{B}\cdot\hat{n})_{mn}$ in different machines is required to produce more precise estimates.

The tolerance for each mode can be defined as the maximal allowed external field at its maximum, divided by the toroidal field at magnetic axis, $B_{t0}\sim 5.3T$. For the symmetric part $C(\theta)$ of the first mode, this is the maximal allowed external field at the outboard midplane divided by $B_{t0}\sim 5.3T$. With this definition, the tolerances are $12/5.3\times10^{-4}\sim 2.2\times10^{-4}$ for the first $n=1$ mode and $18/5.3\times10^{-4}\sim 3.6\times10^{-4}$ for the first $n=2$ mode when $n_e\sim 10^{19}m^{-3}$, based on the assumed scaling $(\delta\vec{B}\cdot\hat{n})_{mn}\sim 10\,Gauss\ n_e(10^{19}m^{-3})$. The tolerances will increase linearly with density. Higher modes will be difficult to control, but their tolerances are not demanding. Figure 7 shows the tolerances for each mode and for $n=1$ to 4 toroidal harmonics. If the advanced scenario is not considered, then the expected tolerances are more optimistic by a factor of 4. Given a set of correction coils and intrinsic field errors, one can roughly estimate required currents in correction coils to reduce the amplitude of the first mode at the outboard midplane below the tolerances. More precise treatment will be investigated by coupling the dominant mode to coil currents when coils and errors are specified.

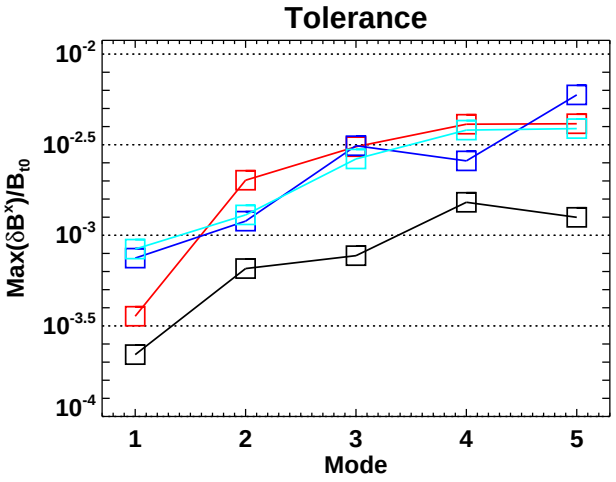

FIG. 7: Tolerances in a log scale, defined as the maximal allowed external field at the outboard midplane divided by the toroidal field at magnetic axis, $B_{t0}\sim 5.3T$, to avoid locking for $n=1$ (black), $n=2$ (red), $n=3$ (blue) and $n=4$ (light blue) toroidal harmonics.

IV. SUMMARY

The IPEC code shows that the effects of external magnetic field errors in ITER can be mitigated by error correction coils that have currents that are fixed to the currents in the basic coil set. The basic method is to identify the distributions of external normal magnetic field to which ITER is most sensitive in any of its planned operating scenarios. The use of correction coils that can ensure that the three most dominant field distributions has no external drive would greatly reduce the sensitivity of ITER to error fields. This is illustrated by the size of of the singular values in Fig. 5 (a) and maximal allowed field in Fig. 7. These distributions are large near the outboard midplane, so error field correction coils should be installed in that region to efficiently produce a compensating external field.

Acknowledgments

This work was supported by DOE contract DE-AC02-76CH03073 (PPPL), DE-FC02-04ER54698 (GA), and DE-FG02-03ERS496 (CU).

APPENDIX: LOCALIZATION OF THE DOMINANT EXTERNAL FIELD

The localization of the dominant mode, or the first mode, corresponds to a broad poloidal harmonic coupling

in toroidal plasmas. Although the dominant mode is described by the external normal magnetic field ($\delta\vec{B}^x \cdot \hat{n}_b$) in the paper, here the corresponding total normal magnetic field ($\delta\vec{B} \cdot \hat{n}_b$) will be considered first. The IPEC computation shows that the plasma is highly perturbed when the total field on the plasma boundary ($\delta\vec{B} \cdot \hat{n}_b$) has a large amplitude in a Fourier component (m_b, n) corresponding to an *effective* safety factor $q_b = m_b/n \sim q_{edge}$. The q_{edge} is the q value at the plasma boundary, which can be taken by the well-defined last closed flux surface inside the separatrix. This is typically $\psi/\psi_{max} \lesssim 0.99$ as in stability calculations, since ideal MHD description in magnetic coordinates becomes inaccurate beyond this point. This resonant behavior occurs with other poloidal Fourier components broadly near m_b in toroidal plasmas due to the strong poloidal coupling. So, the dominant total field on the plasma boundary is given by

$$\delta\vec{B} \cdot \hat{n}_b = \sum_{m \sim m_b \pm \delta m_b} A_{mn} e^{i(m\theta - n\varphi)}, \tag{A.1}$$

in magnetic coordinates. The phases of A_{mn} have to be almost equal to avoid cancelations. This implies that the dominant total field has the cosine factor $\delta\vec{B} \cdot \hat{n_b} \propto \sum_{m_b \pm \delta m_b} cos(m\theta)$ at $\varphi = 0$. In a toroidal configuration, δm_b is wide enough for phase mixing except the only one period $m_b\theta = \pi$ at a specific location, which is the outboard midplane when $\varphi = 0$. Therefore, if one observes the resulting distribution on a poloidal plane at a fixed polar toroidal angle ϕ, the characteristic width can be defined by

$$W_c = \int_{-\pi/2m_b}^{\pi/2m_b} d\theta \frac{B_P}{\vec{B} \cdot \vec{\nabla}\theta}, \tag{A.2}$$

where B_P is the poloidal field. The equation shows that the width W_c is primarily a function of m_b or $q_b = m_b/n$, and other geometric parameters.

The width W_c can be evaluated on Hamada coordinates [21] with $\psi = V$, where V is the enclosed volume, $\mathcal{J} = (2\pi)^{-2}$ as

$$W_c = \int_{-\pi/2m_b}^{\pi/2m_b} d\theta \frac{|\vec{\nabla}V|}{4\pi^2 R}, \tag{A.3}$$

since $B_P = |\vec{\nabla}V|/R$ and $\vec{B} \cdot \vec{\nabla}\theta = 1/\mathcal{J}$, where R is the distance from the toroidal axis. A simple elongated plasma with a Shafranov shift Δ_s has the volume approximately as

$$V(r, \eta) \cong \frac{2\pi^2 r^2 R_0 \kappa}{(1 - \Delta_s cos\eta)^2 (1 + (\kappa^2 - 1) sin^2\eta)}, \tag{A.4}$$

where κ is the elongation, Δ_s is the Shafranov shift normalized by r and (r, η) are the polar coordinates from the magnetic axis $R = R_0$. Since η is a small parameter in the outboard region, $|\vec{\nabla}V|$ is approximately

$$|\vec{\nabla}V| \cong \left|\frac{dV}{dr}\right| = \frac{4\pi^2 r R_0 \kappa}{(1 - \Delta_s)^2}. \tag{A.5}$$

Since $R \approx R_0$ and $r \approx a$ when θ is small, Eq. (A.3) with (A.5) gives

$$W_c \approx \frac{\pi a \kappa}{m_b (1 + \epsilon)(1 - \Delta_s)^2}, \tag{A.6}$$

where ϵ is the inverse aspect ratio. Using a simple scaling $\Delta_s \approx \epsilon$, it is rewritten as

$$W_c \approx \frac{\pi a \kappa}{m_b (1 - \epsilon^2)(1 - \epsilon)}. \tag{A.7}$$

The external field that produces the near-resonant components of the total field has typically higher Fourier components $m_b^x \cong m_b + \delta^x$ due to different propagations [14, 16]. The shift and broad coupling of Hamada poloidal harmonics around a high m_b^x can be seen in Fig. 3. Using the shift in Hamada coordinates, the characteristic width of the external field is given by

$$W_c^x \approx \frac{\pi a \kappa}{m_b^x (1 - \epsilon^2)(1 - \epsilon)}. \tag{A.8}$$

This is a good approximation when the m_b^x is sufficiently high. For instance, the first mode of scenario 4 for (a) $n = 1$ has the peak at $m_b^x = 9$ which is shifted by $\delta^x \approx 3$ from $m_b = q_b n \approx 6$. Since the ITER equilibrium typically has $a \approx 2.0m$, $\kappa \approx 1.8$ and $\epsilon \approx 0.3$, so Eq. A.8 estimates the width by $2m$, as can be roughly read in Fig. 2. The decrease of the width for higher q_b and n can be also seen in Fig. 2.

[1] C. G. Gimblett and R. J. Hastie, Phys. Plasmas **11**, 1019 (2004).

[2] A. Bondeson, Y. Q. Liu, D. Gregoratto, C. M. Fransson, B. Lennartson, C. Breitholtz, Y. Gribov, and V. D. Pustovitov, Phys. Plasmas **9**, 2044 (2002).

[3] T. E. Evans, R. A. Moyer, P. R. Thomas, J. G. Watkins, T. H. Osborne, J. A. Boedo, E. J. Doyle, M. E. Fenstermacher, K. H. Finken, R. J. Groebner, et al., Phys. Rev. Lett. **92**, 235003 (2004).

[4] T. C. Hender, R. Fitzpatrick, A. W. Morris, P. G. Carolan, R. D. Durst, T. Eddlington, J. Ferreira, S. J. Fielding, P. S. Haynes, J. Hugill, et al., Nucl. Fusion **32**, 2091 (1992).

[5] R. Fitzpatrick, Nucl. Fusion **33**, 1049 (1993).

[6] R. Fitzpatrick, Phys. Plasmas **5**, 3325 (1998).
[7] R. J. La Haye, R. Fitzpatrick, T. C. Hender, A. W. Morris, J. T. Scoville, and T. N. Todd, Phys. Fluids B **4**, 2098 (1992).
[8] R. J. Buttery, M. D. Benedetti, D. Gates, Y. Gribov, T. Hender, R. La Haye, P. Leahy, J. Leuer, A. Morris, A. Santagiustina, et al., Nucl. Fusion **39**, 1827 (1999).
[9] J. T. Scoville and R. J. LaHaye, Nucl. Fusion **43**, 250 (2003).
[10] R. J. Buttery, M. DéBenedetti, T. C. Hender, and B. D. Tubbing, Nucl. Fusion **40**, 807 (2000).
[11] S. M. Wolfe, I. H. Hutchinson, R. S. Granetz, J. Rice, A. Hubbard, A. Lynn, P. Phillps, T. C. Hender, D. F. Howell, R. J. La Haye, et al., Phys. Plasmas **12**, 056110 (2005).
[12] J. E. Menard, M. G. Bell, R. E. Bell, E. D. Fredrickson, D. A. Gates, S. M. Kaye, B. P. LeBlanc, R. Maingi, D. Mueller, S. A. Sabbagh, et al., Nucl. Fusion **43**, 330 (2003).
[13] T. C. Hender, J. C. Wesley, J. Bialek, A. Bondeson, A. H. Boozer, R. J. Buttery, A. Garofalo, T. P. Goodman, R. S. Granetz, Y. Gribov, et al., Nucl. Fusion **47**, S128 (2007).
[14] J.-K. Park, M. J. Schaffer, J. E. Menard, and A. H. Boozer, Phys. Rev. Lett. **99**, 195003 (2007).
[15] A. H. Glasser and M. S. Chance, Bull. Am. Phys. Soc. **42**, 1848 (1997).
[16] J.-K. Park, A. H. Boozer, and A. H. Glasser, Phys. Plasmas **14**, 052110 (2007).
[17] M. S. Chance, Phys. Plasmas **4**, 2161 (1997).
[18] A. H. Boozer and C. Nührenberg, Phys. Plasmas **13**, 102501 (2006).
[19] K. C. Shaing, Phys. Rev. Lett. **87**, 245003 (2001).
[20] M. Shimada, D. J. Campbell, V. Mukhovatov, M. Fujiwara, N. Kirneva, K. Lackner, M. Nagami, V. D. Pustovitov, N. Uckan, and J. Wesley, Nucl. Fusion **47**, S1 (2007).
[21] S. Hamada, Nucl. Fusion **2**, 23 (1962).

The Princeton Plasma Physics Laboratory is operated
by Princeton University under contract
with the U.S. Department of Energy.

Information Services
Princeton Plasma Physics Laboratory
P.O. Box 451
Princeton, NJ 08543

Phone: 609-243-2750
Fax: 609-243-2751
e-mail: pppl_info@pppl.gov
Internet Address: http://www.pppl.gov